Global Rice Paddy Inventory (GRPI): a high-resolution inventory of methane emissions from rice agriculture based on Landsat satellite inundation data

Zichong Chen[1*], Haipeng Lin[1], Nicholas Balasus[1], Andy Hardy[2], James D. East[1], Yuzhong Zhang[3], Benjamin R. K. Runkle[4], Sarah E. Hancock[1], Charles A. Taylor[5], Xinming Du[6], Bjoern Ole Sander[7], and Daniel J. Jacob[1]

[1]John A. Paulson School of Engineering and Applied Sciences, Harvard University, Cambridge, MA, USA

[2]Department of Geography and Earth Sciences, Aberystwyth University, Aberystwyth, United Kingdom

[3]Institute of Advanced Technology, Westlake Institute for Advanced Study, Hangzhou, Zhejiang, China

[4]Department of Biological & Agricultural Engineering, University of Arkansas, Fayetteville, AR, USA

[5]John F. Kennedy School of Government, Harvard University, Cambridge, MA, USA

[6]Department of Economics, National University of Singapore, Singapore

[7]International Rice Research Institute (IRRI), Los Baños, Philippines

*Correspondence to: Zichong Chen (zchen1@g.harvard.edu)

This is a non-peer reviewed preprint submitted to *EarthArXiv*. This paper is being submitted to *Earth's Future* for peer review.

Abstract. Rice agriculture is a major source of atmospheric methane, but current emission inventories are highly uncertain, mostly due to poor rice-specific inundation data. Inversions of atmospheric methane observations can help to better quantify rice emissions but require high-resolution prior information on the location and timing of emissions. Here we use Landsat satellite data at 30 m resolution to identify flooded vegetation and combine this information with a 30 m global cropland database, rice-specific data, and a recent global dataset of emission factors (EFs) per unit of rice paddy area. The resulting Global Rice Paddy Inventory (GRPI) provides methane emission estimates at 0.1°× 0.1° (~10 km ×10 km) spatial resolution and monthly resolution. Evaluation of GRPI with independent rice area data and FLUXNET-CH_4 eddy flux measurements shows good agreement. Our global emission of 39.3 ± 4.7 Tg a^{-1} for 2022 (best estimate and error standard deviation) is higher than previous inventories that use outdated rice maps and IPCC-recommended EFs now considered too low. GRPI shows the largest discrepancy from previous inventories in South Asia, where rice agriculture has rapidly developed but outdated rice maps fail to represent it. China is the largest rice emitter in GRPI (8.2 ± 1.0 Tg a^{-1}), followed by India (6.5 ± 1.0 Tg a^{-1}), Bangladesh (5.7 ± 1.2 Tg a^{-1}), Vietnam (5.7 ± 1.0 Tg a^{-1}), and Thailand (4.4 ± 0.9 Tg a^{-1}). These five countries together account for 78% of global total rice emissions. The seasonality of emissions varies between countries depending on local climate and cultivation practices. We define a rice methane intensity (methane emission per unit of rice produced) to assess the potential of mitigating methane without compromising food security. We find national methane intensities ranging from 10 to 120 kg methane per ton of rice produced (global mean 51) for major rice-growing countries. Countries can achieve low intensities with high-yield cultivars, upland rice agriculture, water management, and organic matter management.

1. Introduction

Rice is a staple food for more than half of the world's population, and rice paddies cover 170 million ha or 1.3% of the global land surface. Flooded anoxic conditions combined with a high organic load and standing vegetation make rice paddies a large seasonal source of methane (CH_4), a potent greenhouse gas (US EPA, 2019). Here we use Landsat satellite data combined with rice-specific data to produce a new global gridded (0.1° × 0.1°) inventory of methane emissions from rice agriculture with monthly resolution. The Global Rice Paddy Inventory (GRPI) provides a basis for interpreting atmospheric observations of methane, particularly from satellites, to better quantify methane emissions from rice agriculture and distinguish them from other sectors.

Rice agriculture is concentrated in East, South, and Southeast Asia. These three regions contributed 90% of global rice production in 2022 (FAOSTAT, 2024). The rest is distributed in Africa, the US, South America, and southern Europe. Flooding for rice paddies is seasonal, governed by rice cultivation cycles. Bottom-up estimates of methane emissions from rice agriculture apply emission factors to rice paddy areas over the rice growing season (IPCC, 2006). Upland rice agriculture, where the fields are not flooded, emits negligible methane (Minami and Neue, 1994). Bottom-up methane emission inventories compiled by the Global Carbon Project (GCP) give global rice emissions of 24.6-37.7 Tg a^{-1} for the 2008–2017 decade, accounting for 6-11% of total anthropogenic emissions of methane (Saunois et al., 2020). Rice emission from China, the world's largest rice producer, ranges from 5.3 to 14.2 Tg a^{-1} in these inventories. Rice

is considered to have the largest methane mitigation potential in South and Southeast Asia compared to other sectors (Shindell et al., 2024).

Top-down emission estimates by inversion of satellite observations of atmospheric methane can help to improve bottom-up inventories by using these inventories as prior information (Jacob et al, 2016). High spatial resolution is required in the bottom-up inventory to enable interpretation of the observed atmospheric concentration gradients. Top-down studies generally use the Emissions Database for Global Atmospheric Research (EDGAR; Crippa et al., 2024) inventory as prior estimates because it uniquely provides $0.1^o \times 0.1^o$ spatial resolution and monthly temporal resolution. But these studies find rice emissions in EDGAR to have large errors in magnitude and seasonality (Palmer et al., 2021; Yu et al., 2023).

The principal challenge in constructing spatially and temporally resolved rice emission inventories is the availability of inundation data. Previous studies used satellites to map wetland inundation extent (Lehner and Döll, 2004; Arino et al., 2012; Pekel et al., 2016; Muro et al., 2018; Gerlein-Safdi et al., 2021) but with spatial resolutions of 300 m or larger, which is too coarse to resolve rice paddies (Inman and Lyons, 2020). They also did not differentiate between open water and flooded vegetation. Flooded vegetation is the main driver of methane emission because of the large decaying organic pools and the vascular transport of methane through the plants (Rahman and Yamamoto, 2020; Helfter et al., 2022; Kyzivat et al., 2022; Rajendran et al., 2023). Landsat satellite imagery is available that maps open water and flooded vegetation at 30 m resolution (Díaz-Delgado et al, 2016). Using the Landsat data covering the visible, near-infrared (NIR) and shortwave-infrared (SWIR) bands, Hardy et al. (2020, 2023) developed the Tropical Wetland mapping tool (TropWet) that can map inundation extent at 30 m resolution. TropWet has been applied and evaluated over wetlands across Africa including Tanzania, Botswana, Namibia, Zambia and South Sudan. Here we adapt their methods to map rice paddies worldwide.

Emission factors (EFs) are another source of uncertainty in rice emission inventories. EFs are commonly expressed as mean methane emission per unit of rice paddy area during the growing season (IPCC, 2019). National emission inventories reported to the United Nations Framework Convention on Climate Change (UNFCCC; https://unfccc.int/topics/mitigation/resources/registry-and-data/ghg-data-from-unfccc) often rely on IPCC Tier 1 or Tier 2 methods, where Tier 1 uses global defaults and Tier 2 uses country-specific EFs though with limited adjustments from Tier 1 (Wang et al., 2018). Previous studies have underscored the limited field validation and biases in the IPCC-recommended EFs (Ouyang et al., 2023; Reavis et al., 2023; Chen et al., 2024). Nikolaisen et al. (2023) compiled a global dataset from 2301 field measurements and developed a generalized additive model to infer country-specific EFs as a function of local agricultural practices and environmental factors (soil texture, planting method, rice cultivar, water regime, and climate classification). We use the EFs from their work to develop GRPI.

2. Data and Methods

Fig. 1 shows the general schematic for constructing GRPI. We use Landsat imagery for flooded vegetation combined with global cropland datasets to construct a global monthly $0.1^o \times 0.1^o$ (~10 km × 10 km) fractional area map for rice paddy inundation (Sect 2.1). This is then combined

with country-specific EFs from Nikolaisen et al. (2023) including temperature dependence (Sect. 2.2). Our inventory is for 2022 but the methods can be readily applied to other years. Interannual variability of emissions in Asia is found to be less than 8% (Ouyang et al., 2023). Decadal trends can be more important (Anand et al., 2005; Zhang et al., 2022; Wang et al., 2023; Chen et al., 2024).

2.1. Global mapping of rice paddies

We start by applying the TropWet Google Earth Engine (GEE)-based automatic mapping system developed by Hardy et al (2020, 2023) to generate global monthly data on inundated vegetation from Landsat 7, 8, and 9 surface reflectance data at 30 m pixel resolution using six spectral bands including blue (0.45-0.51 μm), green (0.53-0.59 μm), red (0.64-0.67 μm), NIR (0.85-0.88 μm), SWIR1 (1.57-1.65 μm), and SWIR2 (2.11-2.29 μm). We collect images from Landsat 7, 8, and 9 over a month and combine them into one composite image per 30-m pixel by taking the median value of the pixel surface reflectance in each band; doing so reduces noise from clouds and haze (Azzari and Lobell, 2017). We then apply linear spectral unmixing (Gevaert and García-Haro, 2015) to the composite Landsat imagery to determine the per-pixel fractions of water, vegetation, and bare soil. We also calculate the normalized difference water index (NDWI) from the NIR and SWIR reflectance as $\mathrm{NDWI} = (\mathrm{NIR} - \mathrm{SWIR1})/(\mathrm{NIR} + \mathrm{SWIR1})$, a measure of the water content in leaves of plants. Two terrain metrics including slope angle and Height Above Nearest Drainage (HAND), both generated using the 30 m Shuttle Radar Topography Mission (SRTM) Digital Surface Model (DSM) available in GEE (Farr et al., 2007), are used to further discriminate inundated areas from dry areas. Hardy et al. (2023) used this ensemble of six parameters to produce a set of logical rules (ruleset) identifying inundated 30 m pixels and classifying them as open water, emergent vegetation (herbaceous vegetation emerging from water), aquatic vegetation (floating vegetation completely obscuring the water below), or wet soil. We use the ruleset from Hardy et al (2023) as a first guess pixel classification map. The optimal ruleset given in Table 1 is refined for rice paddies as described below. We combine emergent and aquatic vegetation (referred to hereafter as flooded vegetation) as potential rice paddies.

Our next step is to separate flooded crops from natural wetlands in the flooded vegetation category. We use for that purpose the global Landsat-derived rainfed- and irrigated-cropland product (LGRIP30 version 1.2; Teluguntla et al., 2023) at the same 30 m resolution. We further isolate rice paddies from other flooded crops such as taro and cranberries by using the global RiceAtlas dataset (Laborte et al., 2017), which gives rice area in 2725 spatial units ranging from 11 to 129 kha depending on country. This process yields a first guess rice paddy inundation estimate. We then compare the result to the US Department of Agriculture (USDA) Cropland Data Layer (CDL) (Li et al., 2024) for California, which provides on-the-ground annual rice location data at 30 m resolution and with high accuracy (Luman and Tweddale, 2008), and iteratively adjust the ruleset parameters at $0.1^{o} \times 0.1^{o}$ grid resolution to achieve an optimal match. Table 1 lists the optimized parameters. The CDL also includes data for the South-Central US (the other and more extensive rice-growing area in the US), which we reserve for independent error analysis (Sect. 2.3).

Our final rice paddy product is averaged spatially over 0.1° × 0.1° grid resolution and monthly temporal resolution. Such spatial averaging is needed to reduce noise. Each monthly 0.1° × 0.1° grid cell averages from 439 to 138384 (mean of 80410) individual Landsat clear-sky scenes.

2.2. Emission factors

We use country-specific EFs from Nikolaisen et al. (2023) to compute rice emissions per unit of rice paddy area during the rice growing season. Nikolaisen et al. (2023) compiled 2301 rice paddy field measurements globally and developed a generalized additive model to estimate local mean EFs over the rice growing season as a function of soil texture, pre-season water status, growing-season water regime, planting method, rice cultivar, organic amendment, and climate zone. They then applied that model to derive mean EFs for individual countries, given in Table 2. The highest EF is for Vietnam (3.60 kg ha^{-1} d^{-1}) due to widespread application of farmyard manure and continuous flooding (Pandey et al., 2014; Vo et al., 2018, 2020). The lowest EFs are for India (0.95 kg ha^{-1} d^{-1}) due to sandy soils and rice-wheat rotation systems (Nikolaisen et al., 2023), and for the Philippines (0.97 kg ha^{-1} d^{-1}) due to its adoption of dry direct seeding (seeds are sown directly into dry soils) and alternate wetting and drying practices of rice paddies (Government of Philippines, 2014).

Nikolaisen et al. (2023) derived a global mean EF of 1.97 kg ha^{-1} d^{-1}, whereas the IPCC (2006) Tier 1 recommendation is 1.30 kg ha^{-1} d^{-1}, which is also used in EDGARv8. Older inventories have also used lower EFs (Yan et al., 2005; Wang et al., 2018). The Nikolaisen et al. (2023) values are based on considerably more information. For Vietnam, for example, they use data from 36 field sites covering all major rice regions whereas the Wang et al. (2018) model was based on only two sites. Nikolaisen et al (2023) also take into account the effects of soil texture, planting method, and cultivar type, information that is missing from previous inventories.

We added a temperature dependence to the mean growing-season EFs from Nikolaisen et al. (2023) by applying a multiplicative monthly factor $f(T) = \max(1, 2.5^{\frac{T-30}{10}})$ where T is monthly mean soil temperature (°C) from the Climatic Research Unit and Japanese reanalysis dataset (CRU JRA v2.5; Harris et al., 2024), following the Dynamic Land Ecosystem Model (DLEM; Tian et al., 2010). The resulting monthly EF values are then rescaled to match the mean growing-season values from Nikolaisen et al. (2023).

2.3. Error analysis

We estimate the errors on GRPI methane emissions by adding in quadrature the error variances on rice paddy areas and EFs. Fig. 2 shows the spatial distribution of rice paddies over the South-Central US in GRPI compared to the USDA CDL dataset in 2022 (Li et al.,2024). The rice fraction on the 0.1° × 0.1° grid is defined in the CDL as the maximum monthly fraction over the course of the year and we follow this same definition in GRPI for comparison. The CDL is considered to be highly reliable because of its use of on-the-ground information. We accurately identify rice paddy locations including intensive rice-growing regions in East Arkansas and South Louisiana. Our error standard deviation on the rice paddy area fractions is 31% on the 0.1° × 0.1° grid. We estimate a total rice area of 763 kha across the South-Central US, consistent with but 9% lower than the CDL best estimate of 841 ± 92 kha with 11% uncertainty (Luman and

Tweddale, 2008). On the basis of this comparison, we estimate the GRPI error in identifying rice paddy areas as 31% on the 0.1°×0.1° grid and 10% for national to global scales. Many Southeast Asian countries report emissions to the UNFCCC for 2000, which might explain the low values.

Nikolaisen et al. (2023) reported uncertainties on their EF estimates in individual countries as the standard deviations of residuals between their generalized additive model and individual observations. We convert them to relative uncertainties (Table 2) and assume that they apply uniformly to all grid cells within an individual country as well as to the national totals. Nikolaisen et al. (2023) also reported uncertainties for their regional and global mean EFs (Table 2) and we use these values to estimate the GRPI errors for the corresponding totals.

We evaluate the GRPI methane emissions including error estimates by comparing to eddy flux measurements at rice paddy sites from the FLUXNET-CH_4 network (Delwiche et al., 2021). There are six such sites but three of them (IT-Cas, Italy; PH-RiF, Philippines; US-Twt, US) have highly inconsistent seasonality from year to year, likely influenced by experimental manipulations (Knox et al., 2016). Fig. 3 shows results for the three remaining sites in the US, Korea, and Japan. Close agreement is found for the US-HRA/HRC (US) and JP-MSE (Japan) sites in both magnitude and timing. For the KR-CRK (Korea) site, we capture the observed bimodal distribution driven by mid-season drainage followed by intermittent irrigation (Hwang et al., 2020), but the observations show methane emission extending beyond the rice season which could be due to adjacent wetlands.

3. Results and Discussion

3.1. Global spatial and seasonal distributions of emissions

Fig. 4 shows the global annual mean GRPI rice emissions for 2022, totaling 39.3 ± 4.7 Tg a^{-1}. Five countries account for 78% of global rice emissions including China (8.2 ± 1.0 Tg a^{-1}), India (6.5 ± 1.0 Tg a^{-1}), Bangladesh (5.7 ± 1.2 Tg a^{-1}), Vietnam (5.7 ± 1.0 Tg a^{-1}), and Thailand (4.4 ± 0.9 Tg a^{-1}). The US and Brazil contribute 1.2 ± 0.2 and 0.9 ± 0.1 Tg a^{-1} respectively. Italy and Spain contribute 0.17 ± 0.03 and 0.06 ± 0.01 Tg a^{-1} respectively. Egypt contributes 0.23 ± 0.07 Tg a^{-1}. Rice production in Sub-Saharan Africa has been rising rapidly (Chen et al., 2024), where Nigeria and Madagascar are the top emitters contributing 0.66 ± 0.20 and 0.26 ± 0.08 Tg a^{-1} respectively as of 2022.

Fig. 5 further shows the monthly emissions for Asia on the 0.1° × 0.1° grid. The seasonal distribution varies widely which reflects differences in local climate, water management, and rice cropping systems. In regions with single rice cropping, rice emissions typically persist for five to six months, peaking in July-August over East Asia (northern China, Japan, Korea) and in September-November over South and Southeast Asia (western India, eastern Thailand). Subtropical and tropical regions more commonly practice double or triple cropping, where rice emissions can occur over eight months or longer, with diverse seasonality depending on local management practices (mid-season drainage, intermittent irrigation; Qian et al., 2023).

3.2. Comparison with previous inventories

Fig. 6 compares our GRPI for 2022 to previous inventories. The GCP values (from five different bottom-up inventories) are for 2008-2017, and the UNFCCC inventories are from the most recent national reports (https://unfccc.int/topics/mitigation/resources/registry-and-data/ghg-data-from-unfccc). Our global emission estimate of 39.3 ± 4.7 Tg a^{-1} is higher than the 24.6-37.7 Tg a^{-1} range from the GCP and 24.8 Tg a^{-1} from the sum of UNFCCC national reports. Our difference with the GCP is mainly driven by South Asia (India and Bangladesh, discussed in detail in Sect. 3.3), for which the GCP inventories used outdated rice maps for 2000 (Monfreda et al., 2008; Portmann et al., 2010; Ito et al., 2022). Rice production increased by 54% in India and 52% in Bangladesh from 2000 to 2022 (FAOSTAT, 2024), with increasing rice paddy areas.

EDGAR is the only previous rice inventory available with fine spatial resolution and as such is widely used in inversions of atmospheric methane observations. Global rice emissions in EDGARv8 for 2022 (35.2 Tg a^{-1}) are similar to GRPI, but are double the GRPI values for China and half for South Asia (Fig. 6). EDGARv8 spreads emissions over all agricultural land for many countries in South Asia (India, Bangladesh), Southeast Asia (Thailand, Vietnam), and East Asia (China, Korea, Japan). The seasonality in EDGARv8 is uniform within individual countries. For example, rice emissions in EDGARv8 peak in June everywhere over China, in July over Korea and Japan, and in August over India and Bangladesh, whereas the seasonality in GRPI is more complex (Fig. 5). Inversions of satellite observations of atmospheric methane using EDGAR as prior estimates found EDGAR to be too low in South and Southeast Asia, with incorrect seasonality (Palmer et al., 2021; Yu et al., 2023). GRPI is more consistent with these inversion results.

3.3. Emissions in major rice-producing countries

Fig. 7 shows monthly emissions for the top five emitting countries including China, India, Bangladesh, Vietnam, and Thailand. We discuss individual countries in what follows.

Rice emissions in China are estimated at 8.2 ± 1.0 Tg a^{-1} in GRPI, which agrees well with the GCP mean and with the UNFCCC report, but is a factor of two lower than EDGARv8 (Fig. 6). EDGARv8 used an outdated rice map for 2000, ignoring the changes in irrigation, organic manure use, and rotational patterns, as well as the northward shift of rice agriculture in China in the recent two decades (Chen et al., 2013; Saunois et al., 2020; Xin et al., 2020). These changes have decreased rice emissions (Peng et al., 2016; Ouyang et al., 2023). Chinese emissions generally peak in July-September (Fig. 5), but vary in emission season lengths largely reflecting the diverse rice cropping systems across the country.

Rice emissions in India are estimated at 6.5 ± 1.0 Tg a^{-1} in GRPI, higher than 3.4 Tg a^{-1} in the UNFCCC report and 4.1 Tg a^{-1} in EDGARv8 (Fig. 6). There has been rapid development of rice agriculture in India, with national rice production increasing by 54% from 2000 to 2022 (FAOSTAT, 2024). Previous inventories use outdated rice maps for 2000 and thus underestimate rice emissions. Unlike China, where rice farming is dominated by irrigated paddies, India relies largely on rainfall (Devendra, 2012). The Indian summer monsoon, which lasts from June to September and contributes 80% of annual rainfall (Rajendran et al., 2022), dictates the rice growing season. Fields are typically sown in June–July and harvested in November, resulting in high emissions during July-October and low emissions the rest of the year.

Unlike India, Bangladesh shows sustained emissions throughout the year except for December-January. This reflects its widespread multiple rice cropping. Bangladesh's rice emissions are estimated at 5.7 ± 1.2 Tg a^{-1} in GRPI, higher than 0.37 Tg a^{-1} in the UNFCCC report and 2.3 Tg a^{-1} in EDGARv8. Again, previous inventories use outdated rice maps for 2000 ignoring the rapid development of rice agriculture in Bangladesh (52% increase in rice production from 2000 to 2022). The EF of 2.01 kg ha^{-1} d^{-1} (Table 2) is also higher than the IPCC (2006) Tier 1 value of 1.30 kg ha^{-1} d^{-1}. Recent adoption of modern hybrid rice varieties has doubled emissions compared to local varieties because of longer growth period and intensive irrigation practices (Saha et al., 2021). The disparity in emission seasonality between India and Bangladesh, two neighboring South Asian countries with comparable climatic conditions, illustrates the impact of local agricultural practices on rice emission patterns.

Rice emissions in Vietnam are estimated at 5.7 ± 1.0 Tg a^{-1}, evenly distributed over the year and higher than 1.8 Tg a^{-1} in the UNFCCC report and 1.7 Tg a^{-1} in EDGARv8. This higher estimate is largely due to an EF of 3.6 kg ha^{-1} d^{-1} which is the highest in the world (Table 2). A meta-analysis of field studies across North, Central, and South Vietnam (Vo et al. 2020) found an EF more than double the IPCC default, attributed in part to the well-established irrigation system ensuring consistent water supply to rice paddies. For example, the use of high dikes has facilitated multiple rice crops per year in the Mekong Delta floodplain, an intensive rice region in the country (Tran et al., 2018; Arai et al., 2022).

We estimate elevated rice emissions in Thailand from July to November, peaking in October (Fig. 7). This emission seasonality aligns with the monthly normalized difference vegetation index (NDVI) data derived from MODIS satellite imagery (USDA, 2023). We estimate the Thai rice emissions at 4.4 ± 0.9 Tg a^{-1}, higher than 2.3 Tg a^{-1} of EDGARv8, which again may be largely explained by the outdated rice map used in EDGAR ignoring the rapid rice agriculture development in Thailand (33% increase in production from 2000 to 2022; FAOSTAT, 2024).

The study of Nikolaisen et al (2023), along with other previous inventories (Yan et al., 2005; Wang et al., 2018), trained models with measurements and derived mean EFs at country or regional scales with a set of input variables. This methodology has limitations when it comes to accurately representing emissions at finer scales, particularly for countries with diverse soil texture, climatic and management conditions. Future research aimed at assessing finer-scale EFs could help better quantify rice emissions and guide mitigation strategies.

3.4. Achieving methane mitigation without compromising food security

We use the metric of rice methane intensity, defined as the methane emission per unit of rice produced, to assess the potential for achieving methane reduction without compromising food security in rice agriculture. Fig. 8 shows methane intensities for major rice-producing countries. Values are computed from our GRPI rice emission estimates and FAOSTAT national rice production statistics (FAOSTAT, 2024). We find a wide range of methane intensities across countries, from 120 kg methane per ton of rice produced for Cambodia to 10 for the Philippines. The global mean rice methane intensity is 51 kg methane per ton of rice produced. High methane intensities reflect low yields and/or high EFs. For instance, rice yields in Cambodia, Thailand, and Pakistan are 3.5, 3.0, and 3.7 t ha^{-1}, lower than the global mean of 4.7 t ha^{-1} and only half of China's yield of 7.1 t ha^{-1} (FAOSTAT, 2024). Low methane-intensity

countries such as India and the Philippines have low EFs of 0.95 and 0.97 kg ha^{-1} d^{-1} compared to the global default of 1.97 kg ha^{-1} d^{-1}. The low intensity in India is also partly due to widespread upland rice agriculture, which produces negligible methane and is highly water-saving. Upland rice yields are however much lower than lowland (paddy) rice (Liu et al., 2019); developing high-yield upland rice cultivars would effectively decrease methane intensity. Field studies found that alternate wetting and drying irrigation of rice paddies can also reduce rice emissions and not affect yields (Linquist et al., 2015; Runkle et al., 2018). Directly returning straw to paddy fields as a nutrient supply accelerates methane emissions, but applying straw-derived biochar (biomass charcoal) instead reduces emissions and increases yields (Dong et al., 2013; Sriphirom et al., 2021; Wang et al., 2023). More generally, countries can achieve low methane intensities with high-yield cultivars, upland rice agriculture, water management, and organic matter management (Qian et al., 2023).

4.Conclusions

We developed a new Global Rice Paddy Inventory (GRPI) of methane emissions at $0.1^o \times 0.1^o$ (~10 km × 10 km) monthly resolution by combining Landsat satellite imagery for flooded vegetation with crop information and a large database of emission factors (EFs). This inventory is suitable for use in inversions of atmospheric methane observations to serve as prior information and to distinguish rice emissions from other sectors. The inventory together with error standard deviations is publicly available as monthly $0.1^o \times 0.1^o$ files.

The major challenge in constructing rice emission inventories is the availability of inundation data. We built upon the algorithm of Hardy et al. (2020, 2023) using Landsat imagery to map flooded vegetation at 30 m resolution for individual months. Global cropland datasets were applied to isolate rice paddies from natural wetlands and other flooded crops. The rice paddy area maps were then re-gridded to $0.1^o \times 0.1^o$ resolution for better statistics. We applied country-specific EFs per unit of rice paddy area from the Nikolaisen et al. (2023) generalized additive model based on statistical modeling of a very large number of field measurements of rice emissions, and further applied temperature dependences to these EFs. Evaluation of our inventory with independent rice area data for the US and with FLUXNET-CH_4 eddy flux measurements shows good agreement in emission locations, magnitude, and seasonal timing.

We estimate global rice emissions in 2022 to be 39.3 ± 4.7 Tg a^{-1} (best estimate and error standard deviation), higher than national UNFCCC reports totaling 24.8 Tg a^{-1}, and the Global Carbon Project (GCP)'s range of 24.6-37.7 Tg a^{-1} for the 2008-2017 decade. The inventories contributing to the GCP used outdated 2000 rice maps and IPCC-recommended EFs now recognized to be too low. Our estimates diverge the most from GCP in South Asia where rice agriculture has developed rapidly in the past two decades. The spatially resolved EDGARv8 inventory widely used in inversions of atmospheric observations places global emissions at 35.2 Tg a^{-1}, comparable to GRPI in aggregate, but double for China and half for South Asia, again it seems because of an outdated rice map. The EDGARv8 seasonality also appears to be oversimplified.

China is the highest rice emitter in GRPI (8.2 ± 1.0 Tg a^{-1}), followed by India (6.5 ± 1.0 Tg a^{-1}), Bangladesh (5.7 ± 1.2 Tg a^{-1}), Vietnam (5.7 ± 1.0 Tg a^{-1}), and Thailand (4.4 ± 0.9 Tg a^{-1}). These five countries together account for 78% of global emissions. Rice emissions in China generally

peak in July-August, but differ in emission season lengths due to diverse rice cropping systems. Rice emissions in India are high from July to October, dictated by the summer monsoon. Despite sharing similar climatic conditions with India, Bangladesh has high rice emissions through most of the year due to widespread multiple rice cropping practices.

The potential for reducing methane emissions from rice agriculture while not compromising food security can be quantified using a rice methane intensity metric defined as methane emissions per unit of rice produced. Methane intensities in major rice-producing countries vary by one order of magnitude from 10 to 120 kg methane per ton of rice produced , with a global mean of 51. High methane intensities reflect low yields and/or high EFs. High methane-intensity countries including Cambodia, Thailand, and Pakistan have lower-than-average rice yields. Low methane-intensity countries including India and the Philippines have low EFs. Developing high-yield cultivars, upland rice agriculture, water management, and organic matter management are effective avenues for countries to achieve low methane intensities.

Acknowledgement: This work was supported by the NASA Carbon Monitoring System (CMS). This research has also been funded in the framework of UNEP's International Methane Emissions Observatory (IMEO). Benjamin Runkle was supported by the NASA CMS 80NSSC21K1002. We thank Profs. Zhao Zhang and Zutao Ouyang for their helpful input on Asian rice.

Data and Code Availability: Eddy flux measurement data in the FLUXNET-CH_4 network is available at https://fluxnet.org/data/fluxnet-ch4-community-product/. Methane emission estimates from the Global Carbon Project are available at https://www.icos-cp.eu/GCP-CH4/2019. The Food and Agriculture Organization database (FAOSTAT) is available at https://www.fao.org/faostat/en/#data/QCL. The Landsat satellite imagery and algorithms to support the derivation of inundation extent is archived in Google Earth Engine platform: https://code.earthengine.google.com/a26113fc38b1eb2557e2d39f61ca41e3. Our gridded $0.1^o \times 0.1^o$ GRPI inventory with associated uncertainty will be publicly available at Harvard Dataverse.

Author contributions. ZC and DJJ contributed to the study conceptualization. ZC and HL conducted the data and analysis with contributions from DJJ and NB. ZC and DJJ wrote the paper with input from all authors.

Competing interests. The authors declare that they have no conflict of interest.

References

Anand, S., Dahiya, R. P., Talyan, V., & Vrat, P (2005). Investigations of methane emissions from rice cultivation in Indian context. *Environment International*, **31,** 469-482. https://doi.org/10.1016/j.envint.2004.10.016.

Arai, H., Le Toan, T., Takeuchi, W., Oyoshi, K., Fumoto, T., & Inubushi, K. (2022). Evaluating irrigation status in the Mekong Delta through polarimetric L-band SAR data assimilation. *Remote Sensing of Environment*, **279**, https://doi.org/10.1016/j.rse.2022.113139, 113139.

Arino, O., Ramos Perez, J. J., Kalogirou, V., Bontemps, S., Defourny, P., & Van Bogaert (2012), E. Global land cover map for 2009 (GlobCover 2009), http://efaidnbmnnnibpcajpcglclefindmkaj/https://pdf.usaid.gov/pdf_docs/PA00T2QG.pdf.

Azzari, G., & Lobell, D. B. (2017). Landsat-based classification in the cloud: An opportunity for a paradigm shift in land cover monitoring. *Remote Sensing of Environment*, *202*, 64-74. https://doi.org/10.1016/j.rse.2017.05.025Get rights and content.

Chen, H., Zhu, Q. A., Peng, C., Wu, N., Wang, Y., Fang, X., ... & Yu, G. (2013). Methane emissions from rice paddies natural wetlands, lakes in China: synthesis new estimate. *Global change biology*, **19**(1), 19-32. https://doi.org/10.1111/gcb.12034.

Chen, Z., Balasus, N., Lin, H. et al. (2024). African rice cultivation linked to rising methane. *Nat. Clim. Chang*. **14**, 148–151. https://doi.org/10.1038/s41558-023-01907-x.

Crippa, M., Guizzardi, D., Pagani, F., Schiavina, M., Melchiorri, M., Pisoni, E., Graziosi, F., Muntean, M., Maes, J., Dijkstra, L., Van Damme, M., Clarisse, L., and Coheur, P (2024). Insights into the spatial distribution of global, national, and subnational greenhouse gas emissions in the Emissions Database for Global Atmospheric Research (EDGAR v8.0*), Earth Syst. Sci. Data*, **16**, 2811–2830, https://doi.org/10.5194/essd-16-2811-2024.

Delwiche, K. B., Knox, S. H., Malhotra, A., Fluet-Chouinard, E., McNicol, G. et al. (2021). FLUXNET-CH_4: a global, multi-ecosystem dataset and analysis of methane seasonality from freshwater wetlands, *Earth Syst. Sci. Data*, **13**, 3607–3689, https://doi.org/10.5194/essd-13-3607-2021.

Deng, Z., Ciais, P., Tzompa-Sosa, Z. A., Saunois, M., Qiu, C., Tan, C., Sun, T., Ke, P., Cui, Y., Tanaka, K., Lin, X., Thompson, R. L., Tian, H., Yao, Y., Huang, Y., Lauerwald, R., Jain, A. K., Xu, X., Bastos, A., Sitch, S., Palmer, P. I., Lauvaux, T., d'Aspremont, A., Giron, C., Benoit, A., Poulter, B., Chang, J., Petrescu, A. M. R., Davis, S. J., Liu, Z., Grassi, G., Albergel, C., Tubiello, F. N., Perugini, L., Peters, W., and Chevallier, F (2022). Comparing national greenhouse gas budgets reported in UNFCCC inventories against atmospheric inversions, *Earth Syst. Sci. Data*, **14**, 1639–1675, https://doi.org/10.5194/essd-14-1639-2022.

Devendra, C. (2012). Rainfed areas and animal agriculture in Asia: the wanting agenda for transforming productivity growth and rural poverty. *Asian-Australasian journal of animal sciences*, **25**(1), p.122. 10.5713/ajas.2011.r.09.

Díaz-Delgado, R., Aragonés, D., Afán, I., & Bustamante, J (2016). Long-term monitoring of the flooding regime and hydroperiod of Doñana marshes with Landsat time series (1974–2014). Remote Sensing, **8**(9), 775, https://doi.org/10.3390/rs8090775.

Dong, D., Yang, M., Wang, C., Wang, H., Li, Y., Luo, J., & Wu, W. (2013). Responses of methane emissions and rice yield to applications of biochar and straw in a paddy field. *Journal of Soils and Sediments*, **13**, 1450-1460. https://doi.org/10.1007/s11368-013-0732-0.

US EPA (2019). Global Non-CO2 Greenhouse Gas Emission Projections & Mitigation Potential: 2015-2050, https://www.epa.gov/sites/default/files/2019-09/documents/epa_non-co2_greenhouse_gases_rpt-epa430r19010.pdf.

FAO: FAOSTAT Emissions Land Use database, Food and Agriculture Organization of the United Nations. Statistical Division (2024), available at: http://www.fao.org/faostat/en/#data/GL.

Farr, Tom G., Paul A. Rosen, Edward Caro, Robert Crippen, Riley Duren, Scott Hensley, Michael Kobrick et al (2007). "The shuttle radar topography mission." *Reviews of geophysics*, **45**, no. 2. https://doi.org/10.1029/2005RG000183.

Gerlein-Safdi, C., Bloom, A. A., Plant, G., Kort, E. A., & Ruf, C. S (2021). Improving representation of tropical wetland methane emissions with CYGNSS inundation maps. *Global Biogeochemical Cycles*, **35**(12), e2020GB006890. https://doi.org/10.1029/2020GB006890.

Gevaert, C. M., & García-Haro, F. J. (2015). A comparison of STARFM and an unmixing-based algorithm for Landsat and MODIS data fusion. *Remote sensing of Environment*, *156*, 34-44. https://doi.org/10.1016/j.rse.2014.09.012.

Government of Philippines (2014). Second national communication of the united nations Framework convention on climate change, https://unfccc.int/documents/139241.

Gupta, P.K., Gupta, V., Sharma, C., Das, S.N., Purkait, N., Adhya, T.K., Pathak, H., Ramesh, R., Baruah, K.K., Venkatratnam, L. and Singh, G. (2009). Development of methane emission factors for Indian paddy fields and estimation of national methane budget. *Chemosphere*, **74**(4), pp.590-598. https://doi.org/10.1016/j.chemosphere.2008.09.042.

Hardy, A., Oakes, G., & Ettritch, G (2020). Tropical wetland (TropWet) mapping tool: the automatic detection of open and vegetated waterbodies in Google Earth engine for tropical wetlands. Remote Sensing, **12**(7), 1182, https://doi.org/10.3390/rs12071182.

Hardy, A., Palmer, P. I., & Oakes, G (2023). Satellite data reveal how Sudd wetland dynamics are linked with globally-significant methane emissions. *Environ. Res. Lett.*, **18**(7), 074044, https://doi.org/10.1088/1748-9326/ace272.

Harris, I.C. (2024): CRU JRA v2.5: A forcings dataset of gridded land surface blend of Climatic Research Unit (CRU) and Japanese reanalysis (JRA) data. NERC EDS Centre for

Environmental Data Analysis, *date of citation*. https://catalogue.ceda.ac.uk/uuid/38715b12b22043118a208acd61771917.

Helfter, C., Gondwe, M., Murray-Hudson, M., Makati, A., Lunt, M. F., Palmer, P. I., & Skiba, U (2022). Phenology is the dominant control of methane emissions in a tropical non-forested wetland. *Nature communications*, **13**(1), 133, https://doi.org/10.1038/s41467-021-27786-4.

Houweling, S., Bergamaschi, P., Chevallier, F., Heimann, M., Kaminski, T., Krol, M., Michalak, A. M., and Patra, P (2017).: Global inverse modeling of CH_4 sources and sinks: an overview of methods, *Atmos. Chem. Phys*., **17**, 235–256, https://doi.org/10.5194/acp-17-235-2017.

Hwang, Y., Ryu, Y., Huang, Y., Kim, J., Iwata, H., & Kang, M. (2020). Comprehensive assessments of carbon dynamics in an intermittently-irrigated rice paddy. *Agricultural and Forest Meteorology*, **285**, 107933. https://doi.org/10.1016/j.agrformet.2020.107933.

Inman, V. L., & Lyons, M. B. (2020). Automated inundation mapping over large areas using Landsat data and Google Earth Engine. *Remote Sensing*, **12**(8), 1348. https://doi.org/10.3390/rs12081348.

IPCC: 2006 IPCC guidelines for national greenhouse gas inventories, prepared by the national greenhouse gas inventories program, in: Vol. 2, chap. 4, edited by: Eggleston, H. S., Buendia, L., Miwa, K., Ngara, T., and Tanabe, K. (2006), Institute for Global Environmental Strategies (IGES) on behalf of the IPCC, Hayama, Japan, https://www.ipcc-nggip.iges.or.jp/public/2006gl/index.html.

IPCC, 2019 refinement to the 2006 IPCC guidelines for National Greenhouse gas Inventories, in Vol. 4, Chap. 5, edited by Calvo Buendia, K. Tanabe, A. Kranjc, J. Baasansuren, M. Fukuda, A. Osako, Y. Pyrozhenko, P. Shermanau, & S. Federici (2019), chrome-extension://efaidnbmnnnibpcajpcglclefindmkaj/https://www.ipcc-nggip.iges.or.jp/public/2019rf/pdf/4_Volume4/19R_V4_Ch05_Cropland.pdf.

Ito, A., Inoue, S. and Inatomi, M. (2022). Model-based evaluation of methane emissions from paddy fields in East Asia. *Journal of Agricultural Meteorology*, **78**(2), pp.56-65. 10.2480/agrmet.D-21-00037.

Jacob, D. J., Turner, A. J., Maasakkers, J. D., Sheng, J., Sun, K., Liu, X., Chance, K., Aben, I., McKeever, J., and Frankenberg, C. (2016). Satellite observations of atmospheric methane and their value for quantifying methane emissions, *Atmos. Chem. Phys*., **16**, 14371–14396, https://doi.org/10.5194/acp-16-14371-2016.

Janssens-Maenhout, G., Crippa, M., Guizzardi, D., Muntean, M., Schaaf, E., Dentener, F., Bergamaschi, P., Pagliari, V., Olivier, J. G. J., Peters, J. A. H. W., van Aardenne, J. A., Monni, S., Doering, U., Petrescu, A. M. R., Solazzo, E., and Oreggioni (2019), G. D.: EDGAR v4.3.2 Global Atlas of the three major greenhouse gas emissions for the period 1970–2012, *Earth Syst. Sci. Data*, **11**, 959–1002, https://doi.org/10.5194/essd-11-959-2019.

Knox, S. H., Matthes, J. H., Sturtevant, C., Oikawa, P. Y., Verfaillie, J., and Baldocchi (2016), D.: Biophysical controls on interannual variability in ecosystem-scale CO_2 and CH_4 exchange in a California rice paddy, *J. Geophys. Res.-Biogeo.*, **121**, 978-1001, https://doi.org/10.1002/2015jg003247.

Kyzivat, E.D., Smith, L.C., Garcia-Tigreros, F., Huang, C., Wang, C., Langhorst, T., Fayne, J.V., Harlan, M.E., Ishitsuka, Y., Feng, D. and Dolan, W. (2022). The importance of lake emergent aquatic vegetation for estimating arctic-boreal methane emissions. *Journal of Geophysical Research: Biogeosciences*, **127**(6), p.e2021JG006635. https://doi.org/10.1029/2021JG006635.

Laborte, A. G., Gutierrez, M. A., Balanza, J. G., Saito, K., Zwart, S. J., Boschetti, M., ... & Nelson, A (2017). RiceAtlas, a spatial database of global rice calendars and production. Scientific data, **4**(1), 1-10, https://doi.org/10.1038/sdata.2017.74.

Lehner, B., & Döll, P (2004). Development and validation of a global database of lakes, reservoirs and wetlands. Journal of hydrology, **296**(1-4), 1-22, https://doi.org/10.1016/j.jhydrol.2004.03.028.

Lenka, S., Devi, R., Joseph, C.M. and Gouda, K.C. (2022). Effect of large-scale oceanic and atmospheric processes on the Indian summer monsoon. *Theoretical and Applied Climatology*, **147**(3), pp.1561-1576. https://doi.org/10.1007/s00704-021-03896-3.

Li, H., Di, L., Zhang, C., Lin, L., Guo, L., Eugene, G.Y. and Yang, Z. (2024). Automated In-season Crop-type Data Layer Mapping without Ground Truth for the Conterminous United States based on Multisource Satellite Imagery. *IEEE Transactions on Geoscience and Remote Sensing*. doi: 10.1109/TGRS.2024.3361895.

Linquist, B. A., Anders, M. M., Adviento-Borbe, M. A. A., Chaney, R. L., Nalley, L. L., Da Rosa, E. F., & Van Kessel, C. (2015). Reducing greenhouse gas emissions, water use, and grain arsenic levels in rice systems. *Global change biology*, **21**(1), 407-417. DOI: 10.1111/gcb.12701.

Liu, H., Zhan, J., Hussain, S., & Nie, L. (2019). Grain yield and resource use efficiencies of upland and lowland rice cultivars under aerobic cultivation. *Agronomy*, **9**(10), 591. https://doi.org/10.3390/agronomy9100591.

Luman, D. and Tweddale, T. (2008). Assessment and potential of the 2007 USDA-NASS cropland data layer for statewide annual land cover applications. *Technical Report INHS 2008 (49)*. https://core.ac.uk/download/pdf/4826569.pdf.

Maasakkers, J.D., McDuffie, E.E., Sulprizio, M.P., Chen, C., Schultz, M., Brunelle, L., Thrush, R., Steller, J., Sherry, C., Jacob, D.J. and Jeong, S. (2023). A Gridded Inventory of Annual 2012–2018 US Anthropogenic Methane Emissions. *Environmental science & technology*, **57**(43), pp.16276-16288. https://doi.org/10.1021/acs.est.3c05138.

Meijide, A., Gruening, C., Goded, I., Seufert, G. and Cescatti, A. (2017). Water management reduces greenhouse gas emissions in a Mediterranean rice paddy field. *Agriculture, ecosystems & environment*, **238**, pp.168-178. https://doi.org/10.1016/j.agee.2016.08.017.

Minami, K., & Neue, H. U. (1994). Rice paddies as a methane source. *Climatic change*, **27**(1), 13-26. https://doi.org/10.1007/978-94-015-8328-2_3.

Monfreda, C., Ramankutty, N., & Foley, J. A. (2008). Farming the planet: 2. Geographic distribution of crop areas, yields, physiological types, and net primary production in the year 2000. *Global biogeochemical cycles*, **22**(1). https://doi.org/10.1029/2007GB002947.

Muro, J., Strauch, A., Heinemann, S., Steinbach, S., Thonfeld, F., Waske, B., & Diekkrüger, B (2018). Land surface temperature trends as indicator of land use changes in wetlands. *International Journal of Applied Earth Observation and Geoinformation*, **70**, 62-71, https://doi.org/10.1016/j.jag.2018.02.002.

Nikolaisen, M., Cornulier, T., Hillier, J., Smith, P., Albanito, F., & Nayak, D (2023). Methane emissions from rice paddies globally: A quantitative statistical review of controlling variables and modelling of emission factors. *Journal of Cleaner Production*, 137245, https://doi.org/10.1016/j.jclepro.2023.137245.

Ouyang, Z., Jackson, R. B., McNicol, G., Fluet-Chouinard, E., Runkle, B. R., Papale, D., ... & Zhang (2023), Paddy rice methane emissions across Monsoon Asia. *Remote Sensing of Environment*, **284**, 113335, https://doi.org/10.1016/j.rse.2022.113335.

Palmer, P.I., Feng, L., Lunt, M.F., Parker, R.J., Bösch, H., Lan, X., Lorente, A. and Borsdorff, T. (2021). The added value of satellite observations of methane forunderstanding the contemporary methane budget. *Philosophical Transactions of the Royal Society A*, **379**(2210), p.20210106. https://doi.org/10.1098/rsta.2021.0106.

Pandey, A., Vu, D. Q., Bui, T. P. L., Mai, T. L. A., Jensen, L. S., & de Neergaard, A. (2014). Organic matter and water management strategies to reduce methane and nitrous oxide emissions from rice paddies in Vietnam. *Agriculture, ecosystems & environment*, *196*, 137-146. https://doi.org/10.1016/j.agee.2014.06.010.

Park, S., Im, J., Park, S., Yoo, C., Han, H. and Rhee, J. (2018). Classification and mapping of paddy rice by combining Landsat and SAR time series data. *Remote Sensing*, **10**(3), p.447. https://doi.org/10.3390/rs10030447.

Pekel, J.F., Cottam, A., Gorelick, N. and Belward, A.S. (2016). High-resolution mapping of global surface water and its long-term changes. *Nature*, **540**(7633), pp.418-422. https://doi.org/10.1038/nature20584.

Peng, S., Piao, S., Bousquet, P., Ciais, P., Li, B., Lin, X., Tao, S., Wang, Z., Zhang, Y., and Zhou, F. (2016). Inventory of anthropogenic methane emissions in mainland China from 1980 to 2010, *Atmos. Chem. Phys*., **16**, 14545–14562, https://doi.org/10.5194/acp-16-14545-2016.

Peters, C.N., Bennartz, R. and Hornberger, G.M. (2017). Satellite-derived methane emissions from inundation in Bangladesh. *Journal of Geophysical Research: Biogeosciences*, **122**(5), pp.1137-1155. https://doi.org/10.1002/2016JG003740.

Portmann FT, Siebert S, Döll P. (2010): MIRCA2000 - Global monthly irrigated and rainfed crop areas around the year 2000: A new high-resolution data set for agricultural and hydrological modeling. *Global Biogeochemical Cycles*, **24**, GB1011. DOI: 10.1029/2008GB00343.

Qian, H., Zhu, X., Huang, S., Linquist, B., Kuzyakov, Y., Wassmann, R., Minamikawa, K., Martinez-Eixarch, M., Yan, X., Zhou, F. and Sander, B.O. (2023). Greenhouse gas emissions and mitigation in rice agriculture. *Nature Reviews Earth & Environment*, **4**(10), pp.716-732. https://doi.org/10.1038/s43017-023-00482-1.

Qu, Z., Jacob, D. J., Shen, L., Lu, X., Zhang, Y., Scarpelli, T. R., Nesser, H., Sulprizio, M. P., Maasakkers, J. D., Bloom, A. A., Worden, J. R., Parker, R. J., and Delgado, A. L. (2021): Global distribution of methane emissions: a comparative inverse analysis of observations from the TROPOMI and GOSAT satellite instruments, *Atmos. Chem. Phys*., **21**, 14159–14175, https://doi.org/10.5194/acp-21-14159-2021.

Rahman MM, & Yamamoto A, (2020). Methane cycling in paddy field: a global warming Issue, *Agrometeorology*, London: IntechOpen. DOI: 10.5772/intechopen.94200.

Rajendran, S., Park, H., Kim, J., Park, S. J., Shin, D., Lee, J. H., ... & Kim, C. M. (2023). Methane Emission from Rice Fields: Necessity for Molecular Approach for Mitigation. *Rice Science*, https://doi.org/10.1016/j.rsci.2023.10.003.

Rajendran, K., Surendran, S., Varghese, S.J. and Sathyanath, A. (2022). Simulation of Indian summer monsoon rainfall, interannual variability and teleconnections: evaluation of CMIP6 models. *Climate Dynamics*, **58**(9), pp.2693-2723. https://doi.org/10.1007/s00382-021-06027-w.

Reavis, C. W., Reba, M. L., Shults, D. D., & Runkle, B. R. (2023). Assessing the methane mitigation potential of innovative management in US rice production. *Environmental Research Letters*, **18**(12), 124020. DOI 10.1088/1748-9326/ad0925.

Runkle, B.R., Suvočarev, K., Reba, M.L., Reavis, C.W., Smith, S.F., Chiu, Y.L. and Fong, B. (2018). Methane emission reductions from the alternate wetting and drying of rice fields detected using the eddy covariance method. *Environmental science & technology*, **53**(2), pp.671-681. DOI: 10.1021/acs.est.8b05535.

Saha, M.K., Mia, S., Biswas, A.A.A., Sattar, M.A., Kader, M.A. and Jiang, Z. (2022). Potential methane emission reduction strategies from rice cultivation systems in Bangladesh: A critical synthesis with global meta-data. *Journal of Environmental Management*, **310**, p.114755. https://doi.org/10.1016/j.jenvman.2022.114755.

Saito, K., Asai, H., Zhao, D., Laborte, A.G. and Grenier, C (2018). Progress in varietal improvement for increasing upland rice productivity in the tropics. Plant Production *Science*, **21**(3), 145-158, https://doi.org/10.1080/1343943X.2018.1459751.

Saunois, M., Stavert, A. R., Poulter, B., Bousquet, P., Canadell, J. G., Jackson, R. B., Raymonde et al. (2020). The Global Methane Budget 2000–2017, *Earth Syst. Sci. Data*, 12, 1561–1623, https://doi.org/10.5194/essd-12-1561-2020.

Shaw, J. T., Allen, G., Barker, P., Pitt, J. R., Pasternak, D., Bauguitte, S. J. B., ... & Nisbet, E. G. (2022). Large methane emission fluxes observed from tropical wetlands in Zambia. Global Biogeochemical Cycles, 36(6), e2021GB007261, https://doi.org/10.1029/2021GB007261.

Shindell D, Sadavarte P, Aben I, Bredariol TdO, Dreyfus G, Höglund-Isaksson L, Poulter B, Saunois M, Schmidt GA, Szopa S, Rentz K, Parsons L, Qu Z, Faluvegi G and Maasakkers JD (2024). The methane imperative. *Front Sci* 2:1349770. doi: 10.3389/fsci.2024.1349770.

Sriphirom, P., Chidthaisong, A., Yagi, K., Tripetchkul, S., Boonapatcharoen, N., & Towprayoon, S. (2021). Effects of biochar on methane emission, grain yield, and soil in rice cultivation in Thailand. *Carbon Management*, **12**(2), 109-121. https://doi.org/10.1080/17583004.2021.1885257.

Tian, H., Xu, X., Liu, M., Ren, W., Zhang, C., Chen, G., and Lu, C. (2010). Spatial and temporal patterns of CH_4 and N_2O fluxes in terrestrial ecosystems of North America during 1979–2008: application of a global biogeochemistry model, *Biogeosciences*, **7**, 2673–2694, https://doi.org/10.5194/bg-7-2673-2010.

Teluguntla, P., Thenkabail, P., Oliphant, A., Gumma, M., Aneece, I., Foley, D., & McCormick, R (2023). Landsat-derived Global Rainfed and IrrigatedCropland Product @ 30-m (LGRIP30) of the World (GFSADLGRIP30WORLD), distributed by NASA EOSDIS Land Processes DAAC, https://doi.org/10.5067/Community/LGRIP/LGRIP30.001.

Tran, D., Van Halsema, G., Hellegers, P.J., Phi Hoang, L., Quang Tran, T., Kummu, M. and Ludwig, F. (2018). Assessing impacts of dike construction on the flood dynamics of the Mekong Delta. *Hydrology and Earth System Sciences*, **22**(3), pp.1875-1896. https://doi.org/10.5194/hess-22-1875-2018.

Vo, T. B. T., Wassmann, R., Tirol-Padre, A., Cao, V. P., MacDonald, B., Espaldon, M. V. O., & Sander, B. O. (2018). Methane emission from rice cultivation in different agro-ecological zones of the Mekong river delta: seasonal patterns and emission factors for baseline water management. *Soil Science and Plant Nutrition*, **64**(1), 47-58. https://doi.org/10.1080/00380768.2017.1413926.

Vo, T.B.T., Wassmann, R., Mai, V.T., Vu, D.Q., Bui, T.P.L., Vu, T.H., Dinh, Q.H., Yen, B.T., Asch, F. and Sander, B.O. (2020). Methane emission factors from Vietnamese rice

production: pooling data of 36 field sites for meta-Analysis. *Climate*, **8**(6), p.74. https://doi.org/10.3390/cli8060074.

Wang, J., Akiyama, H., Yagi, K., and Yan, X. (2018). Controlling variables and emission factors of methane from global rice fields, *Atmos. Chem. Phys*., **18**, 10419–10431, https://doi.org/10.5194/acp-18-10419-2018.

Wang, J., Ciais, P., Smith, P., Yan, X., Kuzyakov, Y., Liu, S., Li, T. and Zou, J. (2023). The role of rice cultivation in changes in atmospheric methane concentration and the Global Methane Pledge. *Global Change Biology*, **29**(10), pp.2776-2789. https://doi.org/10.1111/gcb.16631.

Xin, F., Xiao, X., Dong, J., Zhang, G., Zhang, Y., Wu, X., ... & Li, B. (2020). Large increases of paddy rice area, gross primary production, and grain production in Northeast China during 2000–2017. *Science of the Total Environment*, **711**, https://doi.org/10.1016/j.scitotenv.2019.135183,135183.

Yan, X., Yagi, K., Akiyama, H., & Akimoto, H (2005). Statistical analysis of the major variables controlling methane emission from rice fields. *Global Change Biology*, **11**(7), 1131-1141, https://doi.org/10.1111/j.1365-2486.2005.00976.x.

Yu, X., Millet, D. B., Henze, D. K., Turner, A. J., Delgado, A. L., Bloom, A. A., and Sheng, J (2023).: A high-resolution satellite-based map of global methane emissions reveals missing wetland, fossil fuel, and monsoon sources, *Atmos. Chem. Phys*., **23**, 3325–3346, https://doi.org/10.5194/acp-23-3325-2023.

Zhang, B., Tian, H., Ren, W., Tao, B., Lu, C., Yang, J., ... & Pan, S. (2016). Methane emissions from global rice fields: Magnitude, spatiotemporal patterns, and environmental controls. *Global Biogeochemical Cycles*, **30**(9), 1246-1263. https://doi.org/10.1002/2016GB005381.

Zhang, Y., Fang, S., Chen, J., Lin, Y., Chen, Y., Liang, R., ... & Peng, S. (2022). Observed changes in China's methane emissions linked to policy drivers. *Proceedings of the National Academy of Sciences*, **119**(41), e2202742119. https://doi.org/10.1073/pnas.220274211.

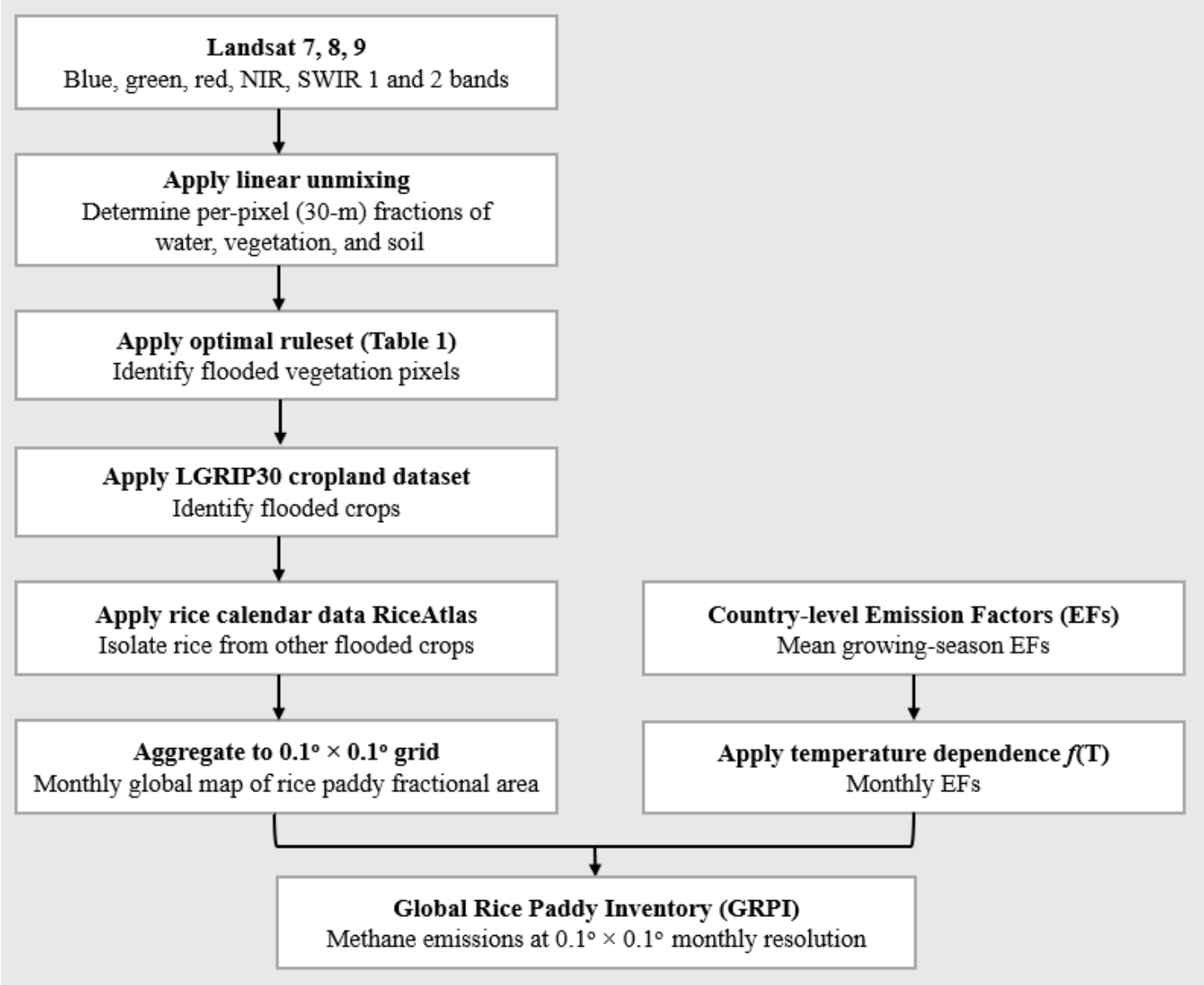

Figure 1. Flowchart for generating the Global Rice Paddy Inventory (GRPI) of methane emissions. NIR and SWIR are near-infrared and short-wave infrared bands respectively. LGRIP30 is the global Landsat-derived rainfed- and irrigated-cropland product at 30 m resolution (Teluguntla et al., 2023).

720

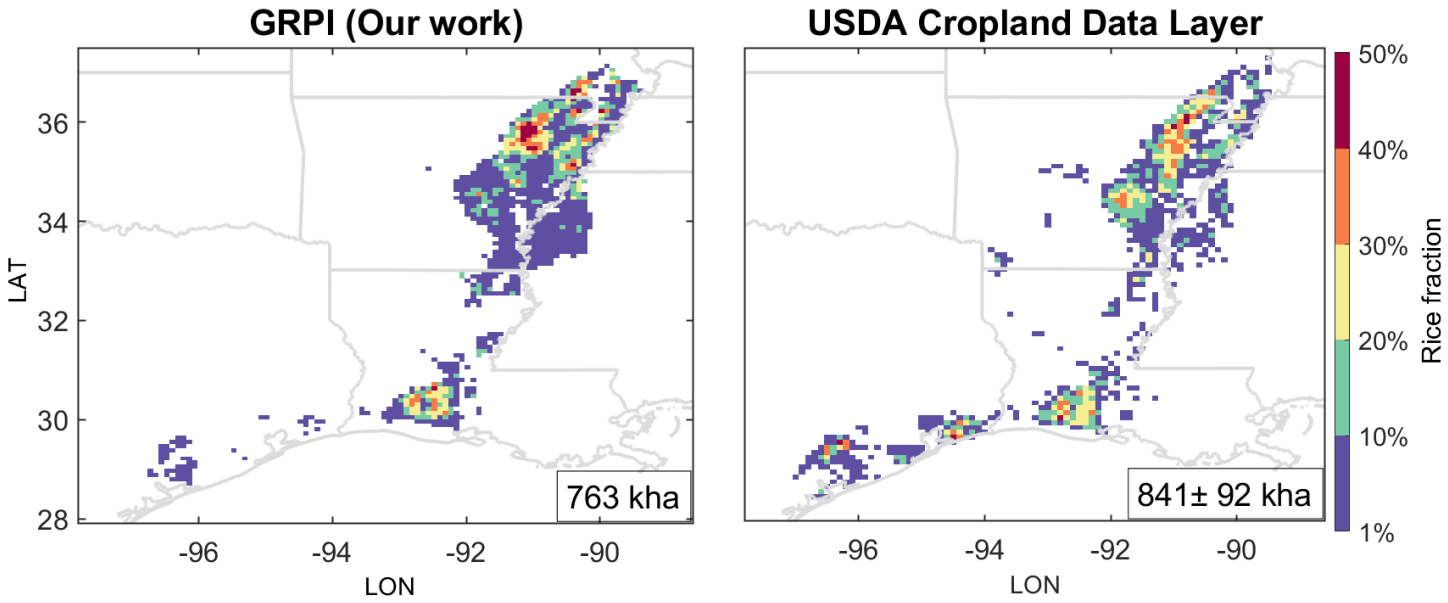

740 **Figure 2**. Rice paddies in the South-Central US in 2022. The spatial distribution in the GRPI (our work) is compared to the Cropland Data Layer (CDL) of the US Department of Agriculture (USDA). The Figure shows the rice paddy fractional areas in $0.1^{o} \times 0.1^{o}$ grid cells. The total rice area in the region is given inset, and the uncertainty in the right panel is estimated from a 11% error assigned to total rice cropland area in the CDL (Luman and Tweddale, 2008).

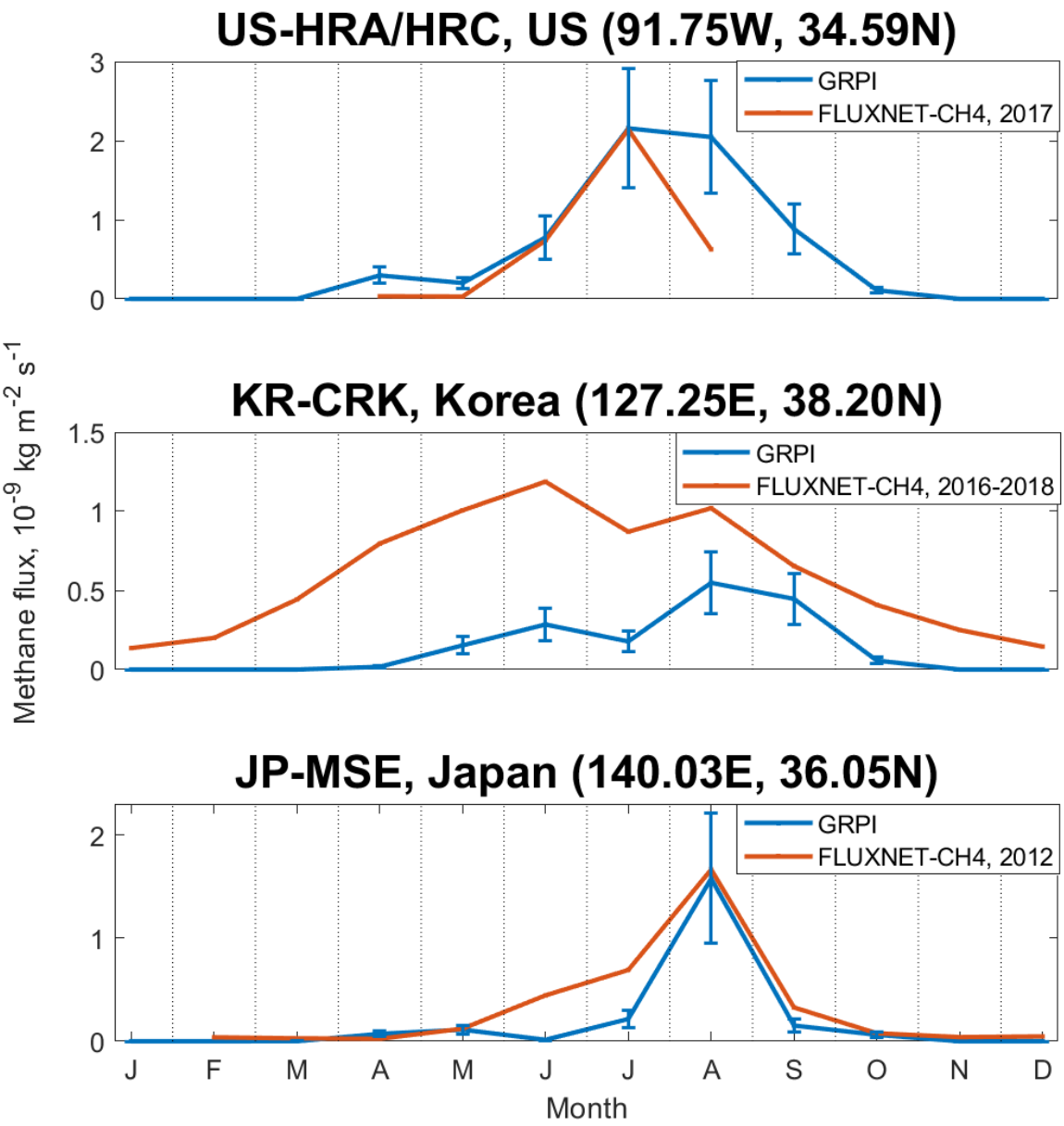

Figure 3. Seasonality of methane emissions at rice paddy sites in the FLUXNET-CH_4 network. Eddy flux measurements at the sites in different years are compared to our GRPI inventory for 2022 on the 0.1°× 0.1° grid. Vertical bars indicate GRPI error standard deviations. The red line in the top panel shows the mean values of two neighboring HRA and HRC sites in Arkansas, US.

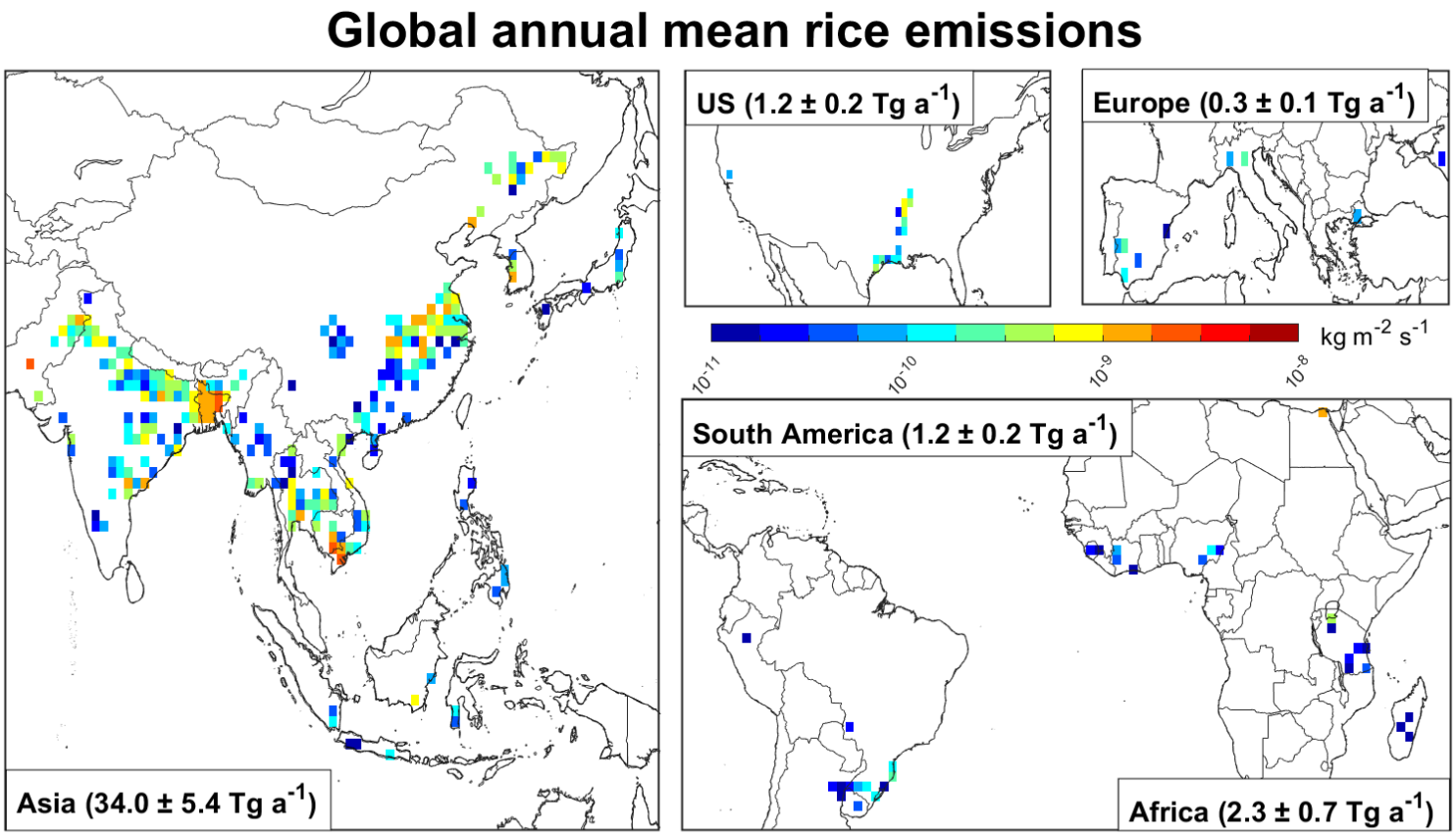

Figure 4. Annual mean rice emissions in 2022 from GRPI in rice-producing regions. The original data at 0.1° × 0.1° resolution are shown as 1.0° × 1.0° averages for visibility. Blank areas have emissions lower than 1×10^{-11} kg m^{-2} s^{-1}. Total emissions with error standard deviations for each region are given inset. National emissions from major rice-growing countries are given in the text.

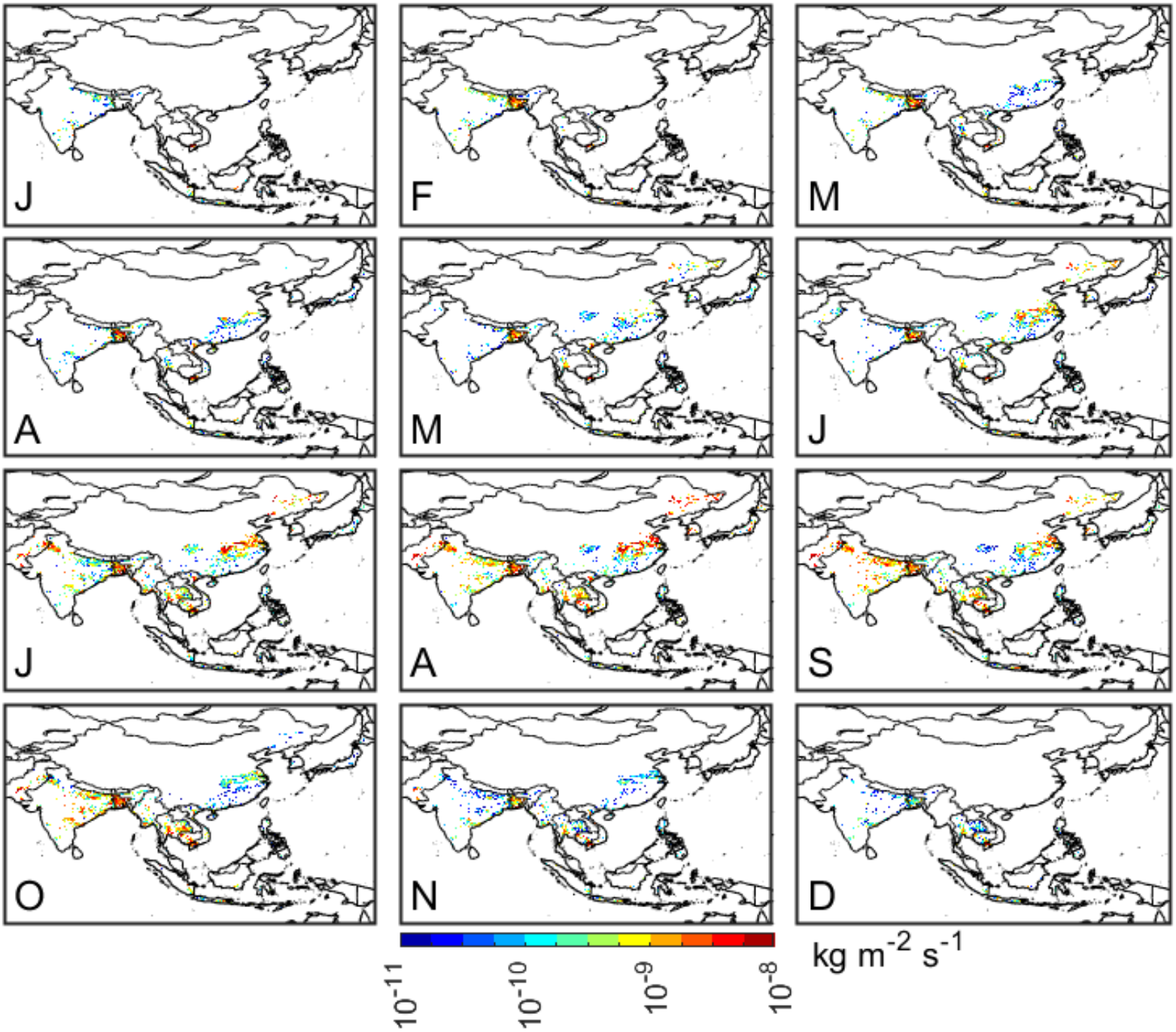

Figure 5. Monthly GRPI rice emissions in Asia at 0.1° × 0.1° grid resolution. Blank areas have emissions lower than 1×10^{-11} kg m^{-2} s^{-1}. Annual mean emissions are shown in Fig. 4, and the seasonalities of national emissions for top emitting countries are shown in Fig. 7.

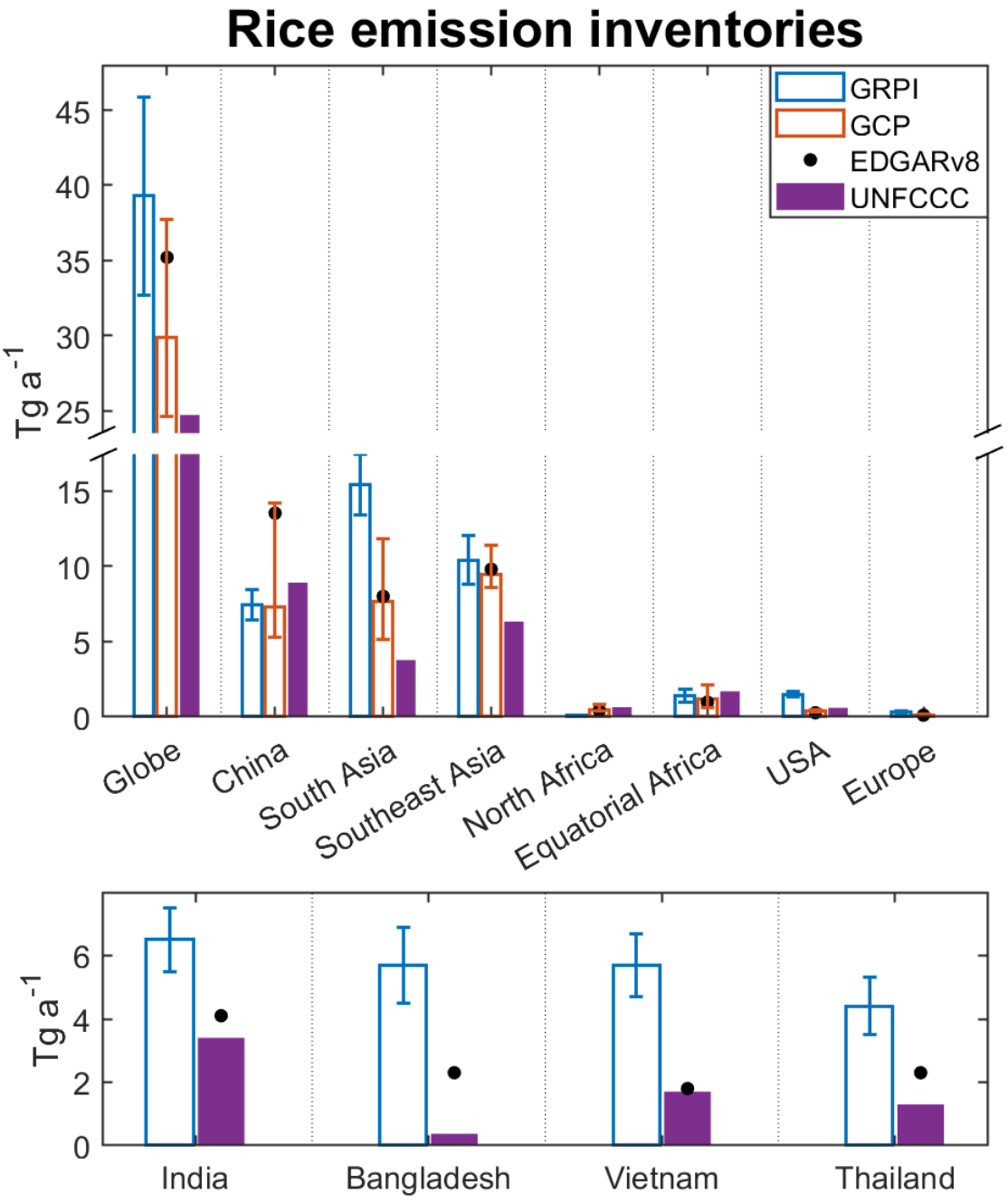

Figure 6. Comparison of our GRPI inventory for 2022 to previous inventories. These include the most recent national reports to the UNFCCC, the EDGARv8 gridded emissions for 2022, and the 2008-2017 mean emissions from five bottom-up inventories contributing to the Global Carbon

Project (GCP): CEDS, EDGARv432, FAO-CH_4, GAINS, and USEPA. Vertical bars for GRPI are error standard deviations. Vertical bars for GCP indicate the range for the five contributing inventories. The regions in the top panel are those resolved by GCP. The bottom panel gives comparisons between GRPI, UNFCCC, and EDGARv8 for additional countries.

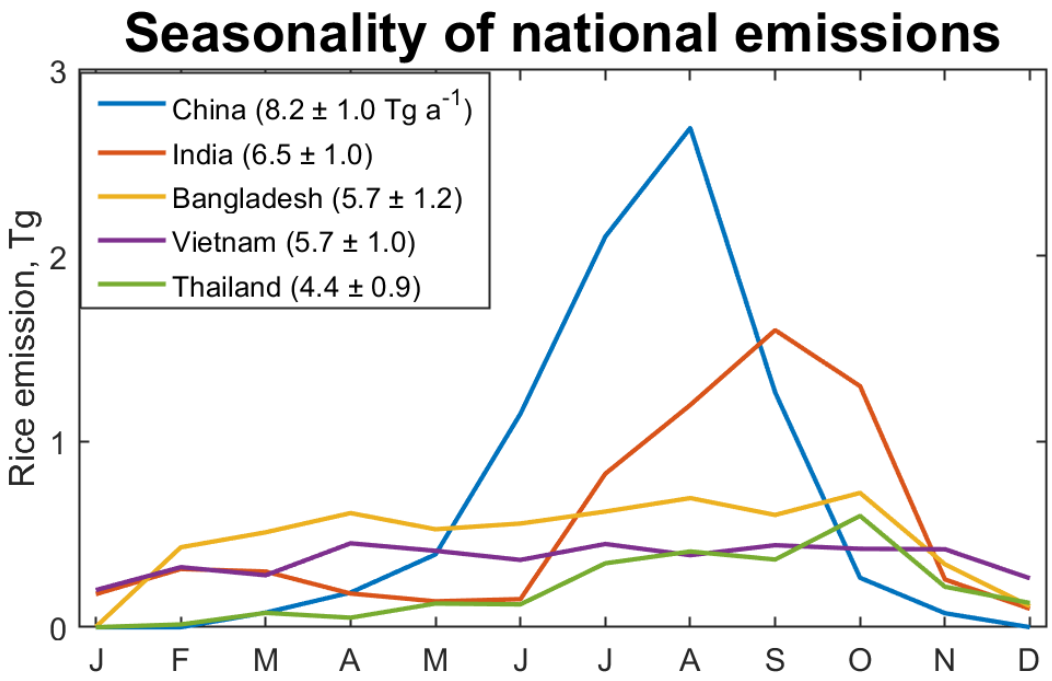

790

Figure 7. Monthly GRPI rice emissions in 2022 for the top five emitting countries. Annual totals with error standard deviations for each country are given inset.

800

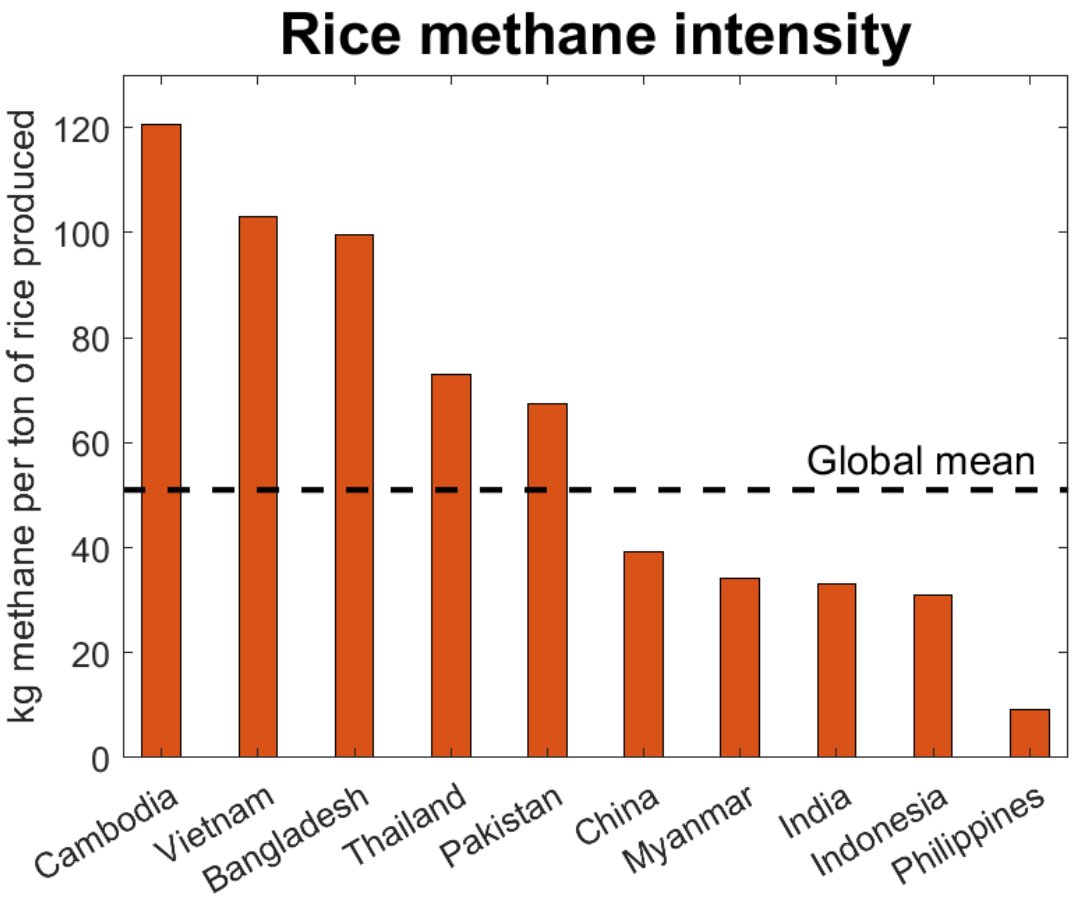

Figure 8. Rice methane intensities (methane emissions per unit of rice produced) in major rice-producing countries for 2022, in units of kg methane per ton of rice produced. Dashed horizonal line indicates the global mean menthane intensity of 51 kg methane per ton of rice produce. Values are computed from our rice emission estimates and FAOSTAT country-specific rice production statistics (FAOSTAT, 2024).

810

820 **Table 1**. Optimal ruleset used for identification of inundated Landsat pixels[a].

Pixel classification	Parameters					
	Water fraction	Vegetation fraction	Bare soil fraction	NDWI[b]	Slope[c]	HAND[c]
Open water	>75%				<2.78%	<30 m
Emergent vegetation	25%-75%	25%-75%			<1.67%	
Aquatic vegetation		>75%		>$NDWI_{p70}$	<1.67%	<15 m
Wet soil	25%-75%		25%-75%		<2.78%	

[a] Parameters from Hardy et al. (2023) with values optimized for rice paddy identification (see text). Pixels with <25% water, excessive slope, and/or excessive HAND are not labeled as inundated. Emergent vegetation and aquatic vegetation categories (referred to together as flooded vegetation) are potential rice paddies if further associated with rice cultivation (see Fig. 1 and text).

[b] Normalized difference water index (NDWI) derived from the Landsat NIR and SWIR radiances as $\mathrm{NDWI} = (\mathrm{NIR} - \mathrm{SWIR1})/(\mathrm{NIR} + \mathrm{SWIR1})$. $NDWI_{p70}$ is the 70^{th} percentile of the NDWI
830 values across pixels within the $0.1^{o} \times 0.1^{o}$ grid cell for each month.

[c] Terrain slope and Height Above Nearest Drainage (HAND) are from the 30-m Shuttle Radar Topography Mission (SRTM) Digital Surface Model (DSM).

840

Table 2. Rice paddy emission factors (EFs) for methane in individual countries and regions[a].

	EF (kg ha^{-1} d^{-1})	Relative uncertainty (%)[b]
Bangladesh	2.08	11.1
Brazil	2.13	4.2
China	2.41	2.1
Ghana	2.54	20.0
India	0.95	5.3
Indonesia	1.96	4.6
Italy	2.21	8.1
Japan	1.53	9.8
Myanmar	1.49	24.2
Philippines	0.97	6.2
Portugal	1.36	33.1
South Korea	2.39	3.3
Spain	2.51	13.1
Thailand	1.27	9.4
Uruguay	1.49	17.4
US	1.25	4.8
Vietnam	3.60	6.7
East Asia	2.03	4.9
South Asia	1.16	6.9
Southeast Asia	1.91	5.2
Europe	2.16	7.4
Africa	2.54	20.0
North America	1.25	4.8
South America	2.04	4.9
World	1.97	2.1

[a] From Nikolaisen et al. (2023).

[b] From the residual standard deviations reported by Nikolaisen et al. (2023) in fitting their generalized additive model to individual measurements in the different countries.